

Pyrolyses of Aromatic Azines: Pyrazine, Pyrimidine, and Pyridine

J. H. Kiefer* and Q. Zhang†

Department of Chemical Engineering, University of Illinois at Chicago, Chicago, Illinois 60607

R. D. Kern,* J. Yao, and B. Jursic

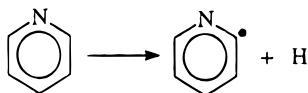
Department of Chemistry, University of New Orleans, New Orleans, Louisiana 70148

Received: January 14, 1997; In Final Form: April 22, 1997[⊗]

The thermal decompositions of pyrazine, pyrimidine, and pyridine in shock waves have been investigated using the complementary techniques of laser-schlieren (LS) densitometry and time-of-flight (TOF) mass spectrometry (1600–2300 K, 150–350 Torr). A free radical chain reaction with initiation by ring C–H fission in the pyrolyses of all three azines is proposed. The measured C–H fission rates are compared and analyzed by RRKM theory. Barriers of 103 ± 2 kcal/mol for pyrazine, 98 ± 2 for pyrimidine, and 105 ± 2 for pyridine have been determined, supporting values lower than the barrier for C–H fission in benzene, 112 kcal/mol. The lower barriers for the azines are explained by the additional contributions of resonance structures of azyl radicals due to neighboring N–C interactions, which serve to further stabilize the azyl radicals. Detailed chain mechanisms are constructed to model the LS profiles and the TOF concentration profiles of the major products, hydrogen cyanide, acetylene, cyanoacetylene, and diacetylene. Of particular interest are the TOF observations and the mechanistic explanation of temperature dependent maxima seen in the formation of cyanoacetylene in the presence or absence of excess H₂.

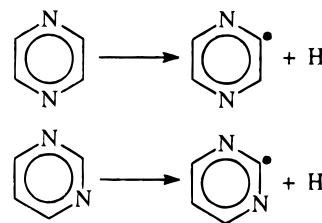
Introduction

An increasing interest is evident in the investigation of the pyrolyses of N-heterocycles containing one or more nitrogen atoms in the aromatic ring such as pyrrole, pyridine, pyrazine, and pyrimidine. This is in large part from their relevance in the formation of various NO_x species during the combustion of heavy oils and of coal. Basic research in this field was first conducted on pyridine with its relative structural simplicity; early studies^{1–7} reported different decomposition rates depending on reaction conditions. These investigations clearly demonstrated the radical chain nature of the decomposition; some studies in fact proposed that the pyrolysis is initiated primarily via C–H fission,^{4–7} most likely from the carbon atom adjacent to the nitrogen atom.⁷



The o-pyridyl radical is believed to be the most stable of the three possible pyridyls and the only major pyridyl radical whose fission leads to the primary decomposition products, HCN, C₂H₂, and CHCCN.⁷ The results of Kern et al. and Mackie et al.^{6,7} also revealed a very low barrier of 93–98 kcal/mol for the initial C–H fission, much lower than the 112 kcal/mol for benzene. The reduced strength of the C–H bond was explained by Kikuchi et al.,⁸ Mackie et al.,⁷ and Jones et al.⁹ as arising from the interaction of the nitrogen lone pair with the neighboring C atom, implying an important chemical effect of the ring N atom and its subsequent effect on the pyrolysis of azines.

The major products of the pyrazine and pyrimidine pyrolyses, HCN, C₂H₂, and CHCCN, were first observed by Doughty et al.^{10,11} in their single-pulse shock-tube studies covering the range 1200–1550 K and a total pressure of 13–14 atm. Both decompositions were considered to be free radical mechanisms initiated by low-barrier C–H fission (~95 kcal/mol), which was again attributed to the effect of the adjacent N–C interaction. A theoretical study by Jones et al.⁹ supports this proposal; however, this predicted somewhat higher barriers of ~104 kcal/mol for the initial dissociations of both molecules.



Doughty et al.^{10,11} reported a greater rate of pyrazine dissociation relative to pyrimidine; this faster rate was ascribed to a rapid abstraction of H atoms from the diazine parents by the CN radical. To account for the difference in the rates, Doughty et al.^{10,11} adopted an “A” factor for the initiation rate in pyrazine which is higher by a factor of ~3 than that for pyrimidine in their model.

An experimental determination of the lower barrier depends critically upon an accurate measurement of initiation rate. In the single-pulse studies^{10,11} of the diazines, initiation rate constants were derived by matching calculated and inferred product yields for various reaction temperatures at the very late times of 600–1000 μs. Here the product yield and distribution will be largely governed by secondary chain processes and thus have but a remote connection to the initiation rate. Moreover,

* Corresponding authors.

† Present address: Department of Chemistry, University of New Orleans.

⊗ Abstract published in *Advance ACS Abstracts*, August 15, 1997.

TABLE 1: Summary of Experimental Conditions

mixture compositions	temperature (K)	pressure (Torr)
	Laser-Schlieren ^a	
4% pyrazine	1689–2362	131–198
	1680–2279	313–342
4% pyrimidine	1679–2301	136–214
	1666–2134	266–349
4% pyridine	1745–2212	107–140
	1722–2272	309–377
	Time-of-Flight ^b	
2% pyrazine	1460–2267	189–376
2% pyrimidine	1491–2216	196–365
2% pyridine	1731–2037	250–322
2% pyrazine–5% H ₂	1641–2158	239–367
2% pyrimidine–5% H ₂	1603–2217	232–382
2% pyridine–5% H ₂	1706–2054	255–334
2% pyridine–5% D ₂	1695–2176	254–372

^a Mixtures balanced by Kr. ^b Diluent consists of 3% Ar balanced by Ne.

kinetic study of such a chain reaction could also be distorted, especially at low temperatures, due to initiation by impurities which more easily release radicals.

The above problems can be most easily avoided by observing the reactions at higher temperatures, where impurities are unimportant and the chain contribution is comparatively minor. To explore the characteristics of the unimolecular initiation and the dynamic formation of its products, a recent study of pyrazine pyrolysis by Kiefer et al.^{12a} was performed at higher temperatures of 1600–2300 K and lower total pressures of 150–350 Torr, utilizing the time-resolved techniques of laser-schlieren (LS) densitometry and time-of-flight mass spectrometry (TOF). This study confirmed the low barriers for both diazine fissions relative to benzene dissociation, but proposed higher values than those reported by Doughty et al.^{10,11} Nonetheless, a nearly doubled barrier reduction was reported for pyrimidine dissociation. With the aid of time-resolved TOF product analysis, an improved pyrazine chain mechanism was constructed featuring a different role of the important chain carrier CN in the formation of one of the key products, cyanoacetylene, CHCCN.

We present here comprehensive mechanisms to describe the pyrolyses for all three azines including in detail the RRKM parameters employed to determine their respective C–H fission barriers. The LS experimental data for pyrazine and pyrimidine^{12a} have been corrected herein for a systematic error (an incorrect calibration factor). The results for all three shock-tube techniques, LS, TOF, and single-pulse, are compared to model calculations using the mechanisms proposed in the present work.

Experimental Section

The experimental apparatus and the procedures for both the LS and TOF techniques have been described previously.^{12a,13} The conditions for the azine experiments are summarized in Table 1; some additional details are as follows.

LS. Pyridine, pyrazine, and pyrimidine were obtained from Aldrich (purity > 99%) and were vacuum degassed; only the middle fractions were retained. Krypton was Spectra-Gases excimer grade. Mixtures were prepared manometrically in a 50 L glass bulb fitted with a Teflon-coated magnetic stirrer, and the uncertainty of mixture composition was less than 1% of the C₅H₅N and C₄H₄N₂ fractions. The molar refractivities of pyrazine and pyrimidine were taken as a constant, 22.73 and 23.44, respectively.¹⁴ Although these must vary during decomposition, the mixture refractivity values are generally >87% from that of Kr. A total of 56 runs of 2% and 4% pyrazine in Kr and 48 runs of 4% pyrimidine in Kr were analyzed. The pyridine data were published previously.⁶

TOF. The chemicals used for the TOF experiments were obtained from several sources: pyrazine, pyrimidine, pyridine (Aldrich, >99%), H₂ (Matheson, >99%), C₂H₂ (Matheson, 99.6%), Ar (Matheson, 99.998%), and Ne (Matheson, 99.999%). Solid pyrazine was sublimed into a gas-handling system and purified by bulb-to-bulb distillation. The middle fraction was retained. A similar procedure was applied to purifying pyrimidine and pyridine vapors. Before the shock-tube experiments, the mixtures were analyzed by the TOF mass spectrometer at room temperature. No impurities were recorded within the static detection limit of the TOF, ca. 300 ppm.

The mass spectrometric calibration factor, also known as the sensitivity factor, for one of the major products observed throughout the TOF experiments, C₂H₂, was measured using a 2% C₂H₂–3% Ar–95% Ne mixture under nonreacting shock conditions. The sensitivity factors for HCN, cyanoacetylene, and diacetylene were determined by nitrogen and carbon atom balances, respectively, during shock experiments.

The recorded mass spectra were transferred from a Tektronix digitizer (RTD720A) to a PC and automatically searched for the mass peaks of interest. The peak heights of preselected masses are stored in a multicolumn data file. The converted concentration profiles are stored in a separate file for the purpose of comparison with modeling results.

Results

Some typical LS semilog gradient profiles for azine dissociation are shown in Figure 1, where the measured density gradient, $d\rho/dx$, is plotted against time. All the azine dissociations can be resolved to ~2300 K; below ~1600 K, the gradients are too small for detection. The most important feature evident in these experiments is that the density gradients all go through a clearly discernible shallow maximum after an initial rise, descending at late time. In our lower to moderate temperature range, this process is more easily resolved than at higher temperatures, where the positions of the maxima are shifted toward $t = 0$ and the initial rise of the density gradients becomes difficult to see. These maxima, often well resolved within the first 5 μ s, are an important indication of chain decomposition which have also been observed in benzene dissociation.¹⁵ As the chain reaction proceeds, the increasing rate of endothermic reaction causes continuously increasing positive density gradients at the early stage of the reactions, whereas at the late times the slow-down from the temperature drop produces negative gradients and thus generates the maxima. This evidence for a chain reaction is consistent with the conclusions of Doughty et al.^{7,10,11} based on their product distribution.

TOF concentration profiles of the major product species from two pyrimidine experiments are displayed in Figure 2. The major product species seen here are HCN, C₂H₂, and CHCCN, the same as those identified in the single-pulse studies of Doughty et al.^{10,11} At high temperatures, C₄H₂ is also detectable in the present study. Mass peaks attributable to cyanogen and acrylonitrile were observed within a concentration range, $(0.1-1) \times 10^{-9}$ mol/cm³, which is within the TOF detection limit. Their detection values are rough upper limit to their amounts formed, although the scatter of the points is too high to construct quantitative reaction profiles.

A 2% C₅D₅N–3% Ar–Ne mixture was analyzed to distinguish the minor products of pyridine pyrolysis. Several species have the same molecular mass in nondeuterated pyridine, for example, C₄H₃ and cyanoacetylene (m/e 51), or C₂N₂ and C₄H₄ (m/e 52). The TOF results revealed that C₄H₃ and C₄H₄ concentrations are negligibly low. Thus, the mass peak m/e 51 observed in

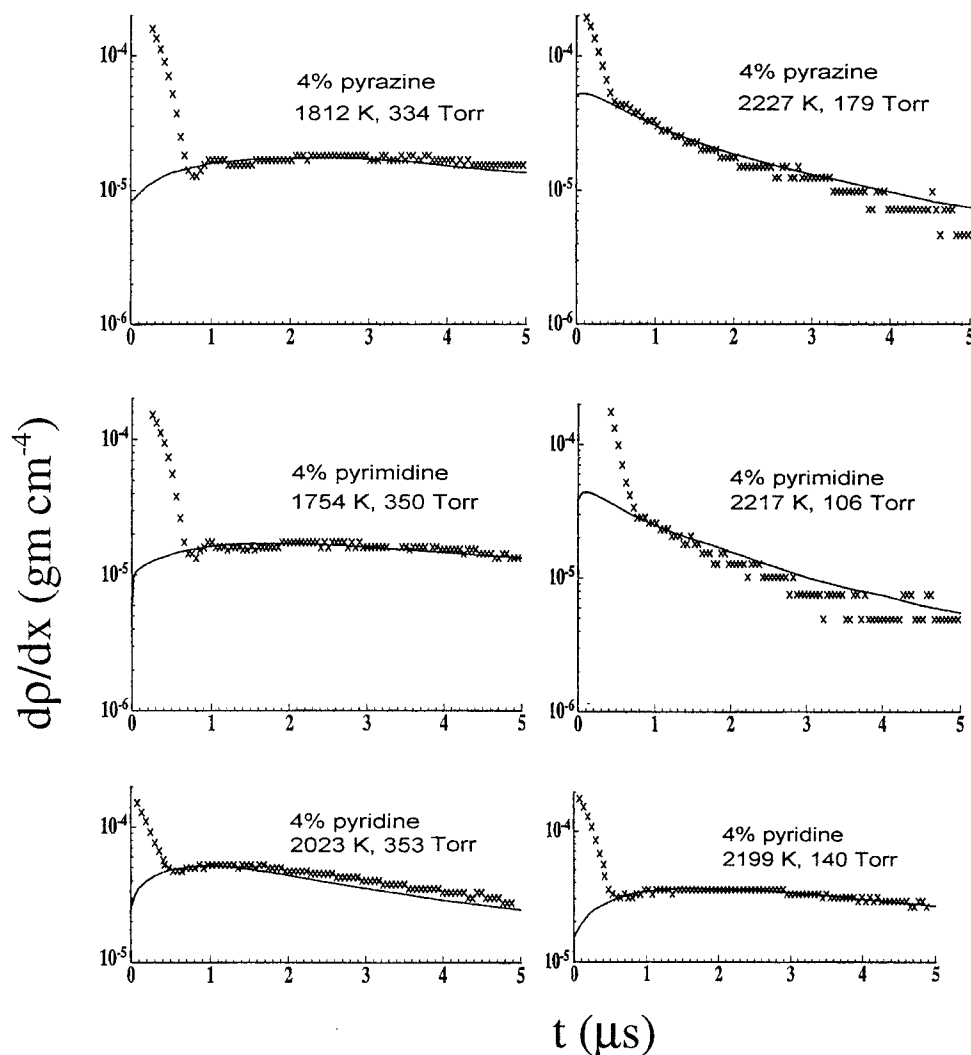


Figure 1. Laser-schlieren semilog density gradient profiles for 4% pyridine/diazine–Kr experiments. Experimental gradients are indicated by the symbol (\times); calculated gradients are shown by the solid lines.

the nondeuterated pyridine experiments is primarily from cyanoacetylene. The mass peaks at m/e 52 and m/e 53 are attributed mostly to the cracking pattern of the parent pyridine. The concentrations of HCN, C_2H_2 , C_4H_2 , and CHCCN at low temperatures all increase monotonically with reaction time and eventually level out, whereas, at high temperatures, CHCCN exhibits a sharp early maximum before a final drop to a constant value.

The effect of hydrogen addition, reducing dramatically the yield of CHCCN for all three azines, is shown in Figure 3. However, this reduction effect is not significant for the other species produced in the reaction.

Thermochemistry

The successful kinetic simulation of the complex free-radical chain revealed by the LS results for all three azines relies on the completeness and accuracy of the thermochemical information of the involved species. As discussed in the Introduction, the proposed stabilization effect due to the interaction between a N atom lone electron pair and a neighboring C atom unpaired electron in the azyl radicals implies that the usual bond-energy methods cannot accurately estimate the energies of these radicals. The C–H bond energies of these azines are regarded here as primary unknowns whose values are to be determined by kinetic modeling and the application of unimolecular rate theory.

Further ring opening and cleavage of the azyl radicals is expected to generate various radicals with acyclic structures containing six to eight carbon and nitrogen atoms with the radical site on the N atom. A group additivity estimation of the heats of formation of these species requires a value for the imine N–H bond dissociation energy D_0 . As in the work on pyrazine pyrolysis,^{12a} we shall adopt a value of 89 kcal/mol, that calculated using density functional theory.^{12b} This value is now found to be fully consistent with the latest *ab initio* calculation by Melius.¹⁶

Another ambiguity arises from the uncertainty of the thermodynamic contribution of the (imine) N_i-C_d group, which is also not available for the group additivity method.¹⁶ In this study its value is assumed to be the same as that of N_i-C_B , recognizing that the same value has been assigned for both the C_d-C_dH and C_d-C_BH groups.¹⁷

The heat of formation of CHCCN was reported as 96 kcal/mol in the pyrazine work,^{12a} based on a matching of the late-time high-temperature CHCCH TOF profiles to modeling calculations. Here the distribution of products is nearly independent of the kinetics of the involved reactions and largely determined by the thermochemistry of the species. The sensitivity of $\Delta_f H^\circ_{298}(\text{CHCCN})$ to the late concentration profile is illustrated in Figure 4. It can be seen that the late-time concentration value would be a factor of ~ 2 too high if a value of 93 kcal/mol was used. Although the $\Delta_f H^\circ_{298}(\text{CHCCN})$

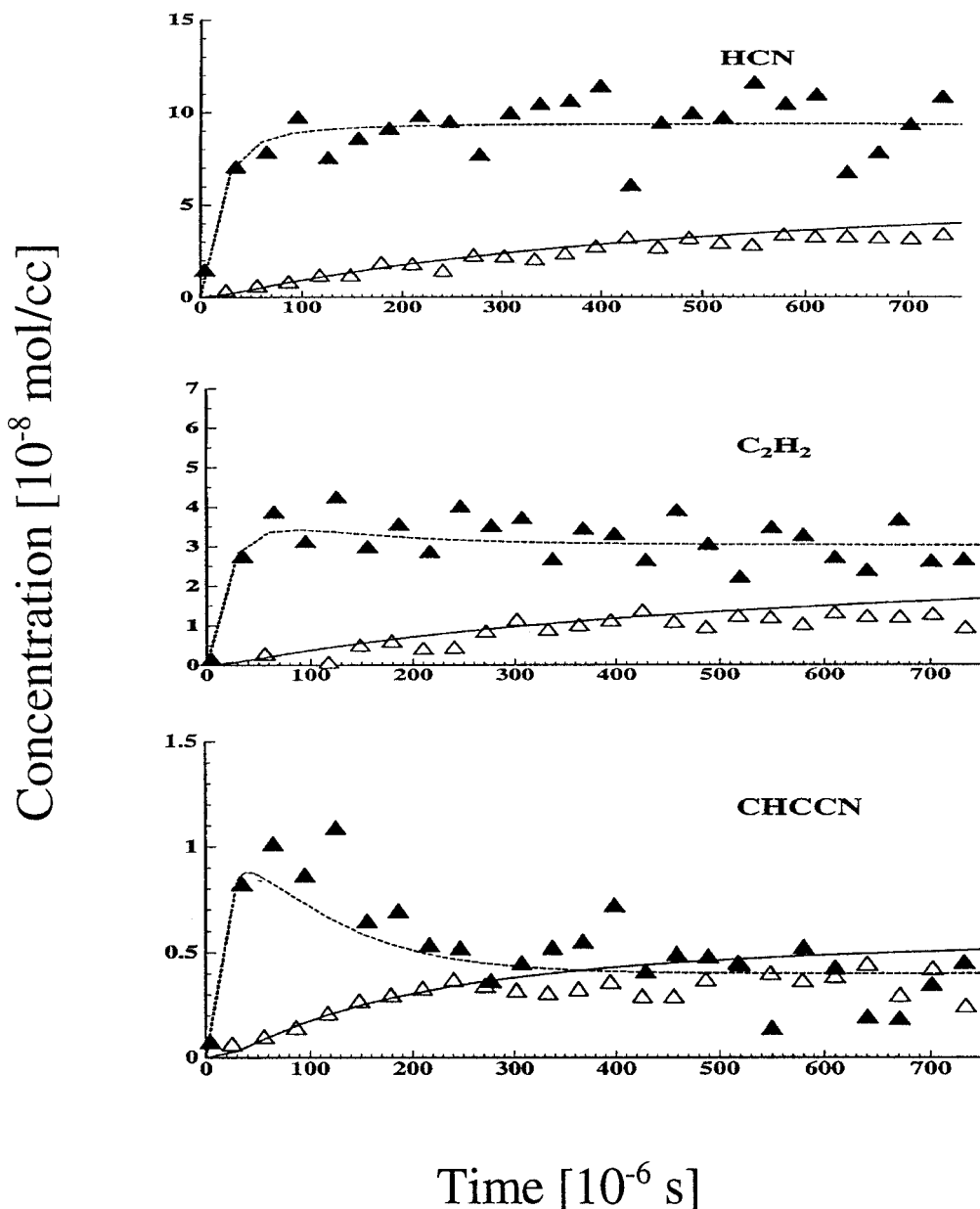


Figure 2. TOF product profiles from two experiments in 2% pyrimidine–3% Ar–Ne at 1635 K, 228 Torr (Δ) and 2042 K, 327 Torr (\blacktriangle). The solid lines show simulations using the mechanism of Table 4.

derived here is indeed higher by ~ 12 kcal/mol than an earlier measurement of 84 reported by Harland,¹⁸ it should be noted that the usual group additivity suggests a value of 91 kcal/mol,¹⁷ which is also consistent with the estimates of 90.8 and 91.3 by Dorofeeva et al.¹⁹ and Dibeler et al.,²⁰ respectively. The reliability of the additivity value essentially depends on the accuracy of the group value C_t –CN, 64 kcal/mol, suggested by Benson¹⁷ from the measured heat of formation of 128.1 kcal/mol for NC–CC–CN ($2C_t$ –CN groups) given by Chu and Stull et al.²¹ All of these indicate that $\Delta_f H^\circ_{298}(\text{CHCCN})$ could well be higher than 90 kcal/mol and therefore partially supports our conclusion.

Some important thermochemical data are listed in Table 2; other properties were estimated from standard statistical thermodynamic formulas.

Kinetics

(1) Initiation Rates. The observed overall shape of the LS azine profiles is indicative of a chain reaction which we assume to be initiated by C–H fission of the parent. The rate constants

for the initial dissociations of the azines are taken directly from the zero-time gradients obtained by extrapolation of the LS profiles using the mechanisms in Tables 3, 4, and 5 (discussed below) to indicate the correct path through the first unresolved microsecond,^{6,15,22} which lies within the induction time for this chain. This procedure of model-assisted extrapolation is particularly important in this work in order to define the zero-time gradients, because in the first few microseconds, the reaction is dominated by chain acceleration.

With a well-described initial rise and location of the maximum, as in Figure 1, the model-assisted extrapolation provides reliable values for $(d\rho/dx)_{t=0}$. To convert these values to rates of initial dissociation, the assumptions of vibrationally relaxed and chemically frozen postincident shock conditions are employed.

First-order rate constants for pyrazine and pyrimidine have been reported.^{12a} A set of new values derived as above, and corrected for a systematic error, are displayed in Figure 5. The systematic error caused slightly lower density gradients by a factor of ~ 1.5 . The present Arrhenius expressions and their

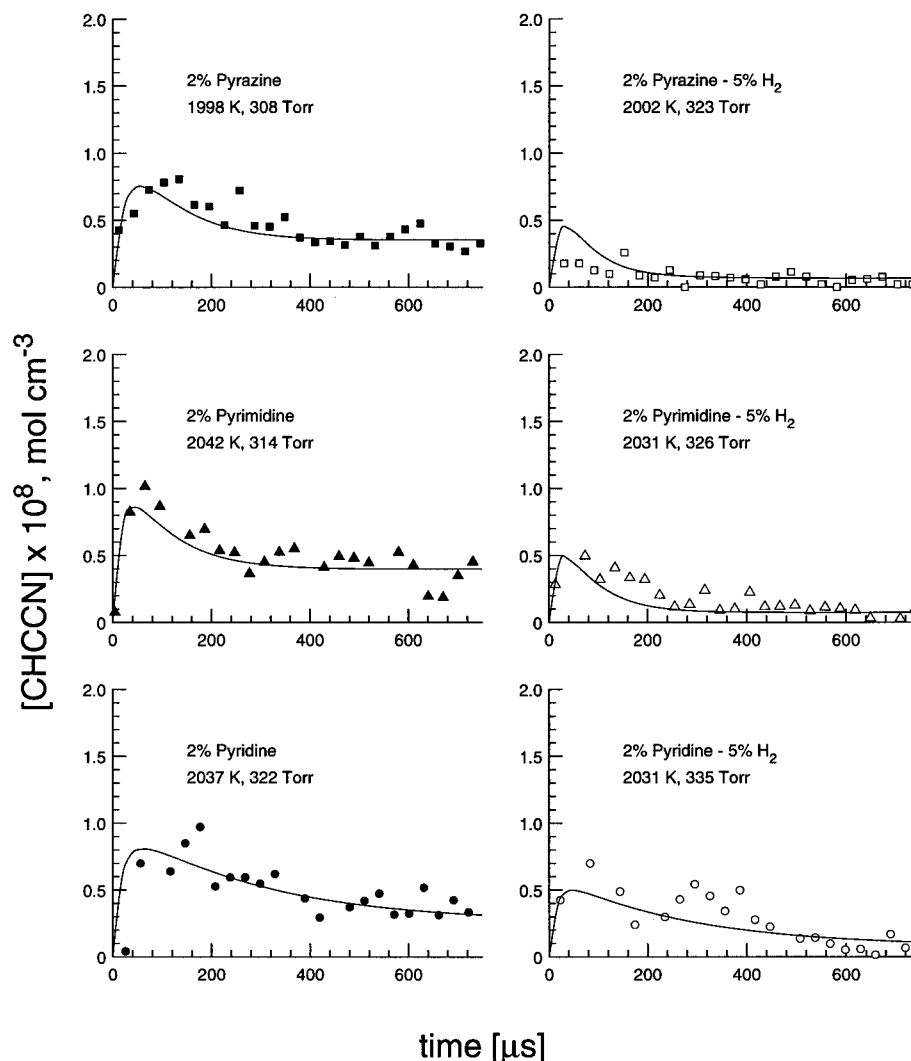


Figure 3. Effect of H₂ addition on the CHCCN profiles for pyrazine, pyrimidine, and pyridine. Solid lines show simulations using the mechanisms of Tables 3, 4, and 5, respectively.

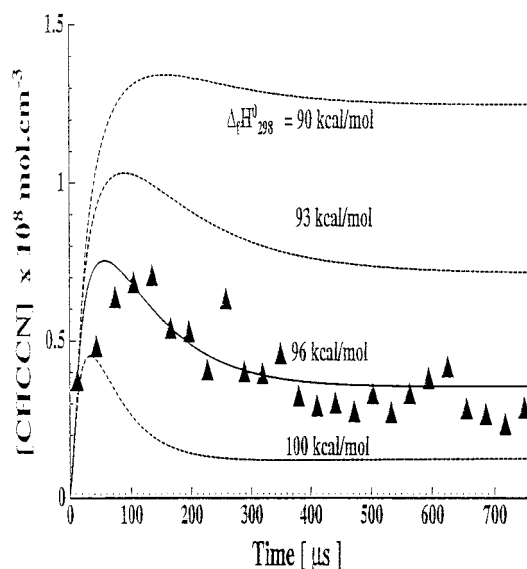


Figure 4. Effect of various values of $\Delta_f H_{298}^\circ$ for cyanoacetylene on the modeling calculations for a 2% pyrazine experiment (\blacktriangle) at 1998 K and 308 Torr.

respective rms values for pyrazine dissociation are as follows:

131–198 Torr

$$k \text{ (s}^{-1}\text{)} = 10^{65.97} T^{-14.72} e^{-124.08(\text{kcal/mol})/RT} \quad (\text{rms } 6.06\%)$$

However, the correction applied herein results in a much better fit of the LS pyrazine and pyrimidine profiles without a change in the mechanism. In fact, the problems with the late-time calculations, noted in ref 12, are no longer present.

313–342 Torr

$$k \text{ (s}^{-1}\text{)} = 10^{56.93} T^{-12.17} e^{-116.84(\text{kcal/mol})/RT} \quad (\text{rms } 2.57\%)$$

The expressions for pyrimidines are

136–214 Torr

$$k \text{ (s}^{-1}\text{)} = 10^{40.46} T^{-8.10} e^{-90.07(\text{kcal/mol})/RT} \quad (\text{rms } 4.91\%)$$

266–349 Torr

$$k \text{ (s}^{-1}\text{)} = 10^{8.84} T^{0.5} e^{-59.32(\text{kcal/mol})/RT} \quad (\text{rms } 5.70\%)$$

Figure 5 clearly exhibits not only a pressure dependence, i.e., falloff behavior for both diazines, but also an evident difference in their initiation rates; pyrimidine dissociation appears faster than pyrazine under similar conditions, and the temperature dependence of the pyrazine rate is stronger than that of pyrimidine. This implies that the initial pyrazine dissociation must have a larger activation energy.

A model-assisted extrapolation of the pyridine LS density gradients to $t = 0$ was also performed on the LS data for pyridine pyrolysis published by Kern et al.,⁶ using the improved

TABLE 2: Important Thermochemical Data in Azine Pyrolyses

species	$\Delta_f H^\circ_{298}$ (kcal/mol)	S_{298} (cal/ (mol K))	ref
C ₄ H ₄ N ₂ (pyrazine)	47.0	65.8	35, 36
C ₄ H ₄ N ₂ (pyrimidine)	46.0	67.2	35, 37
C ₅ H ₅ N (pyridine)	33.5	67.5	6
C ₄ H ₃ N ₂ (pyrazyl)	98.0	69.7	pw ^a and 36
2-C ₄ H ₃ N ₂ (2-pyrimidyl)	92.0	68.5	pw and 37
4-C ₄ H ₃ N ₂ (4-pyrimidyl)	97.0	69.8	pw and 37
5-C ₄ H ₃ N ₂ (5-pyrimidyl)	105.9	69.8	pw and 37
<i>o</i> -C ₅ H ₄ N (<i>o</i> -pyridyl)	86.3	69.4	pw
<i>m,p</i> -C ₅ H ₄ N (<i>m,p</i> -pyridyl)	93.4	69.2	pw
C ₂ N ₂	76.0	57.7	16, 46
HCN	32.3	48.2	46
C ₂ H ₂	54.5	48.0	46
C ₄ H ₂	111.0	59.7	6
C ₄ H ₃	114.0	65.5	pw and 34
CH≡C–CN	96.0	60.1	pw
CH ₂ =CH–CN	43.7	65.3	38
NC–CH=CN	90.6	65.9	pw and 39
CH=CH–CN	102.6	66.2	pw and 38
NC–N=CH	115.3	65.8	pw and 17, 39

^a pw = present work.

mechanism shown in Table 5. The newly derived initial rate constants for pyridine decomposition are found to be ~30% lower than the previous ones and are not affected by the aforementioned systematic error which applies to only the LS pyrazine and pyrimidine data. The modified initiation rates are displayed in Figure 6. The least-squares fits for both

pressures are:

107–140 Torr

$$k \text{ (s}^{-1}\text{)} = 10^{149.62} T^{-37.19} e^{-211.83(\text{kcal/mol})/RT} \quad (\text{rms } 12\%)$$

309–377 Torr

$$k \text{ (s}^{-1}\text{)} = 10^{101.06} T^{-23.98} e^{-165.23(\text{kcal/mol})/RT} \quad (\text{rms } 9\%)$$

These initial rates are found to be generally lower by ~30% than the previous LS results.⁶ However, the LS pyridine data are still modeled satisfactorily by the solid lines as shown in Figure 1.

The results of RRKM analyses of the measured azine initiation rates are also depicted in Figures 5 and 6. The parameters of these calculations, chosen to fit the measured rate constants, are detailed in Table 6. All the models have the usual restricted-rotor Gorin transition state appropriate for bond fission. These calculations assume the same $\langle \Delta E \rangle_{\text{down}} = 400 \text{ cm}^{-1}$ (average $\langle -\Delta E \rangle_{\text{all}} \approx 53 \text{ cm}^{-1}$, for 1500–2300 K) and $\eta = 0.008$ for all three azines, values typical for large hydrocarbons.²³ This indicates the similarity of the reaction and the energy transfer behavior of these large molecules; only the barriers were varied. This value of $\langle \Delta E \rangle_{\text{down}}$ is also supported by Miller and Barker²⁴ in their recent calculation of $\langle -\Delta E \rangle_{\text{all}}$ (~55 cm⁻¹) for pyrazine. Fits to the measured rates in both high- and low-pressure ranges are excellent, with a barrier of $103 \pm 2 \text{ kcal/mol}$ for C–H fission in pyrazine, $98 \pm 2 \text{ kcal/}$

TABLE 3: Reaction Mechanism for Pyrazine Pyrolysis

no.	reaction	A (cgs)	n	E _a (kcal/mol)	ref
Initiation					
(1)	C ₄ H ₄ N ₂ + M = C ₄ H ₃ N ₂ + H + M			---	see text---
Propagation					
(2)	C ₄ H ₃ N ₂ = C ₂ H ₂ + NCCHN	1.00E12 ^a	0.00	30.0	cf. text
(3)	NCCHN + M = CN + HCN + M	3.55E42	-7.73	50.3	RRKM
(4)	NCCHN + M = H + C ₂ N ₂ + M	5.62E37	-6.45	44.1	RRKM
(5)	CN + C ₄ H ₄ N ₂ = 2HCN + CHCHCN	2.00E14	0.00	0.0	cf. text
(6)	CHCHCN + M = C ₂ H ₂ + CN + M	2.57E59	-11.91	84.2	RRKM
(7)	CHCHCN + M = CHCCN + H + M	2.57E46	-8.55	64.0	RRKM
(8)	H + C ₄ H ₄ N ₂ = C ₄ H ₃ N ₂ + H ₂	3.16E12	0.00	0.0	est.
(9)	CN + C ₄ H ₄ N ₂ = HCN + C ₄ H ₃ N ₂	7.94E5	2.30	0.0	41
(10)	CHCHCN + C ₄ H ₄ N ₂ = CH ₂ CHCN + C ₄ H ₃ N ₂	1.00E4	2.40	1.0	est.
(11)	CN + HCN = H + C ₂ N ₂	7.94E7	1.60	0.0	42, est.
(12)	CN + H ₂ = HCN + H	5.49E2	3.20	-0.2	43
(13)	CN + C ₂ H ₂ = CHCCN + H	7.52E22	-3.00	0.0	41, est.
(14)	C ₂ H + HCN = H + CHCCN	7.52E22	-3.00	0.0	41, est.
(15)	C ₂ H + HCN = CN + C ₂ H ₂	9.68E23	-3.00	0.0	41, est.
(16)	C ₂ H + C ₂ H ₂ = C ₄ H ₂ + H	1.2E14	0.00	0.0	44
(17)	CH ₂ CHCN + H = CHCHCN + H ₂	6.61E5	2.50	6.0	45, est.
(18)	CH ₂ CHCN + CN = CHCHCN + HCN	7.94E5	2.30	0.0	41, est.
(19)	H ₂ + C ₂ H = C ₂ H ₂ + H	4.07E5	2.40	0.2	44, est.
(20)	C ₂ H + C ₂ N ₂ = CHCCN + CN	3.16E13	0.00	0.0	est.
Termination					
(21)	H + NCCHN = H ₂ + C ₂ N ₂	3.97E13	0.00	0.0	est.
(22)	H + NCCHN = 2HCN	3.13E13	0.00	0.0	est.
(23)	CN + NCCHN = HCN + C ₂ N ₂	1.00E14	0.00	0.0	est.
(24)	H + CHCHCN = H ₂ + CHCCN	3.97E13	0.00	0.0	est.
(25)	H + CHCHCN = HCN + C ₂ H ₂	3.15E13	0.00	0.0	est.
(26)	H + CHCHCN = CH ₂ CHCN	1.00E12	0.00	0.0	est.
(27)	CN + CHCHCN = HCN + CHCCN	1.00E14	0.00	0.0	est.
(28)	CN + CHCHCN = C ₂ N ₂ + C ₂ H ₂	3.15E13	0.00	0.0	est.
(29)	2CHCHCN = CHCCN + CH ₂ CHCN	3.15E13	0.00	0.0	est.
(30)	NCCHN + CHCHCN = C ₂ N ₂ + CH ₂ CHCN	1.58E13	0.00	0.0	est.
(31)	C ₂ H + CN + M = CHCCN + M	1.99E17	0.00	0.0	est.
(32)	C ₂ N ₂ + M = 2CN + M	7.24E16	0.00	100.3	extrap. 45
(33)	HCN + M = H + CN + M	4.57E15	0.00	105.2	extrap. 45
Molecular Channels					
(34)	CH ₂ CHCN = C ₂ H ₂ + HCN	8.89E11	0.00	68.0	extrap. 45
(35)	CH ₂ CHCN = CHCCN + H ₂	1.26E13	0.00	77.0	extrap. 45

^a Read as 1.00 × 10¹².

TABLE 4: Reaction Mechanism for Pyrimidine Pyrolysis

no.	reaction	A (cgs)	n	E _a (kcal/mol)	ref
Initiation					
(36)	C ₄ H ₄ N ₂ + M = 2-C ₄ H ₃ N ₂ + H + M			---	see text---
Propagation					
(37)	2-C ₄ H ₃ N ₂ = C ₂ H ₂ + NCCHN	2.82E12 ^a	0.00	40.0	cf. text
(38)	4-C ₄ H ₃ N ₂ = HCN + CHCHCN	2.51E11	0.00	30.0	cf. text
(39)	5-C ₄ H ₃ N ₂ = H + HCN + CHCCN	1.00E13	0.00	45.0	cf. text
(40)	NCNCH + M = CN + HCN + M	3.63E27	-3.66	25.6	RRKM
(41)	CN + C ₄ H ₄ N ₂ = HCN = C ₂ H ₂ + NCCHN	1.00E14	0.00	0.0	cf. text
(42)	CN + C ₄ H ₄ N ₂ = 2HCN + CHCHCN	2.00E14	0.00	0.0	cf. text
(43)	H + C ₄ H ₄ N ₂ + H ₂ + 2-C ₄ H ₃ N ₂	1.58E12	0.00	0.0	est.
(44)	H + C ₄ H ₄ N ₂ = H ₂ + 4-C ₄ H ₃ N ₂	3.16E12	0.00	0.0	est.
(45)	H + C ₄ H ₄ N ₂ = H ₂ + 5-C ₄ H ₃ N ₂	1.58E12	0.00	8.0	est.
(46)	CN + C ₄ H ₄ N ₂ = HCN + 2-C ₄ H ₃ N ₂	2.00E5	2.30	0.0	41
(47)	CN + C ₄ H ₄ N ₂ = HCN + 4-C ₅ H ₃ N ₂	3.98E5	2.30	0.0	41
(48)	CN + C ₄ H ₄ N ₂ = HCN + 5-C ₄ H ₃ N ₂	2.00E5	2.30	1.0	41
(49)	CHCHCN + C ₄ H ₄ N ₂ = CH ₂ CHCN + 2-C ₄ H ₃ N ₂	2.51E3	2.40	0.0	est.
(50)	CHCHCN + C ₄ H ₄ N ₂ = CH ₂ CHCN = 4-C ₄ H ₃ N ₂	5.01E3	2.40	3.0	est.
(51)	CHCHCN + C ₄ H ₄ N ₂ = CH ₂ CHCN + 5-C ₄ H ₃ N ₂	2.51E3	2.40	8.0	est.
Termination					
(52)	H + NCNCH = H ₂ + C ₂ N ₂	3.97E13	0.00	0.0	est.
(53)	H + NCNCH = 2HCN	3.15E13	0.00	0.0	est.
(54)	CN + NCNCH = HCN + C ₂ N ₂	1.00E14	0.00	0.0	est.
(55)	NCNCH + CHCHCN = C ₂ N ₂ + CH ₂ CHCN	2.00E13	0.00	0.0	est.

^a Read as 2.82×10^{12} .

TABLE 5: Reaction Mechanism for Pyridine Pyrolysis

no.	reaction	A (cgs)	n	E _a (kcal/mol)	ref
Initiation					
(56)	C ₅ H ₅ N + M = <i>o</i> -C ₅ H ₄ N + H + M			---	see text---
Propagation					
(57)	<i>o</i> -C ₅ H ₄ N = C ₂ H ₂ + CHCHCN	1.00E13 ^a	0.00	50.0	cf. text
(58)	<i>m</i> -C ₅ H ₄ N = C ₄ H ₃ + HCN	3.16E12	0.00	40.0	cf. text
(59)	<i>p</i> -C ₅ H ₄ N = C ₄ H ₃ + HCN	3.16E12	0.00	40.0	cf. text
(60)	C ₄ H ₃ + M = C ₄ H ₂ + H + M	7.67E33	-5.40	37.0	RRKM
(61)	CN + C ₅ H ₅ N = HCN + C ₂ H ₂ + CHCHCN	1.00E14	0.00	0.0	cf. text
(62)	H + C ₅ H ₅ N = <i>o</i> -C ₅ H ₄ N + H ₂	6.31E12	0.00	0.7	est.
(63)	H + C ₅ H ₅ N = <i>m</i> -C ₅ H ₄ N + H ₂	6.31E12	0.00	8.0	est.
(64)	H + C ₅ H ₅ N = <i>p</i> -C ₅ H ₄ N + H ₂	3.15E12	0.00	8.0	est.
(65)	CN + C ₅ H ₅ N = HCN + <i>o</i> -C ₅ H ₄ N	3.98E5	2.30	0.0	est.
(66)	CN + C ₅ H ₅ N = HCN + <i>m</i> -C ₅ H ₄ N	3.98E5	2.30	0.0	est.
(67)	CN + C ₅ H ₅ N = HCN + <i>p</i> -C ₅ H ₄ N	2.00E5	2.30	0.0	est.
(68)	CHCHCN + C ₅ H ₅ N = CH ₂ CHCN + <i>o</i> -C ₅ H ₄ N	5.01E3	2.40	0.0	est.
(69)	CHCHCN + C ₅ H ₅ N = CH ₂ CHCN + <i>m</i> -C ₅ H ₄ N	5.01E3	2.40	5.0	est.
(70)	CHCHCN + C ₅ H ₅ N = CH ₂ CHCN + <i>p</i> -C ₅ H ₄ N	2.51E3	2.40	4.5	est.
Termination					
(71)	H + C ₄ H ₃ = H ₂ + C ₄ H ₂	3.97E13	0.00	0.0	est.
(72)	H + C ₄ H ₃ = 2C ₂ H ₂	1.99E13	0.00	0.0	est.
(73)	CN + C ₄ H ₃ = HCN + C ₄ H ₂	1.00E14	0.00	0.0	est.
(74)	CN + C ₄ H ₃ = CHCCN + C ₂ H ₂	3.15E13	0.00	0.0	est.
(75)	CHCHCN + C ₄ H ₃ = C ₄ H ₂ + CH ₂ CHCN	1.99E13	0.00	0.0	est.

^a Read as 1.00×10^{13} .

mol for pyrimidine, and 105 ± 2 kcal/mol for pyridine. The larger rate and lower E_a of pyrimidine are clearly evident in Figure 5.

(2) Reaction Mechanism. The complete reaction mechanisms used to simulate the LS and TOF data are listed in Table 3 for pyrazine, Table 4 for pyrimidine, and Table 5 for pyridine. Some of the reactions in Table 3, (3)–(7) and (11)–(35), are common to pyrimidine; (6), (7), (11)–(20), (23)–(29), and (31)–(35) are common to pyridine.

In the mechanisms of Tables 3–5, H and CN radicals appear as the two primary chain carriers. The complexity of azine pyrolyses undoubtedly incurs numerous additional species and reactions. However, to adequately explain the kinetic behavior of the major products HCN, C₂H₂, CHCCN, and C₄H₂, it is only necessary to consider a few important reactions whose

origins and rate constants are discussed in the following sections. Other reaction rates are based primarily on literature values or estimates.

Azyl Radical Dissociations. In contrast to the simple, dominant pyrazyl dissociation path indicated by the bold arrow steps in Scheme 1,^{12a} there are three main pathways for pyrimidyl dissociation, all of which are illustrated in Scheme 2 (a–c). Standard heats of reactions (kcal/mol) for the major and minor pathways are in parentheses. In Scheme 2, only (a), (c), and the bold-arrow channels in (b) are included. It should be noted that the heats of reaction of these first azyl ring-opening steps in Schemes 1 and 2 are all < 36 kcal/mol, whereas that of phenyl dissociation, shown in Scheme 3, is almost 62 kcal/mol. This strongly implies much lower barriers for the azyl dissociations.

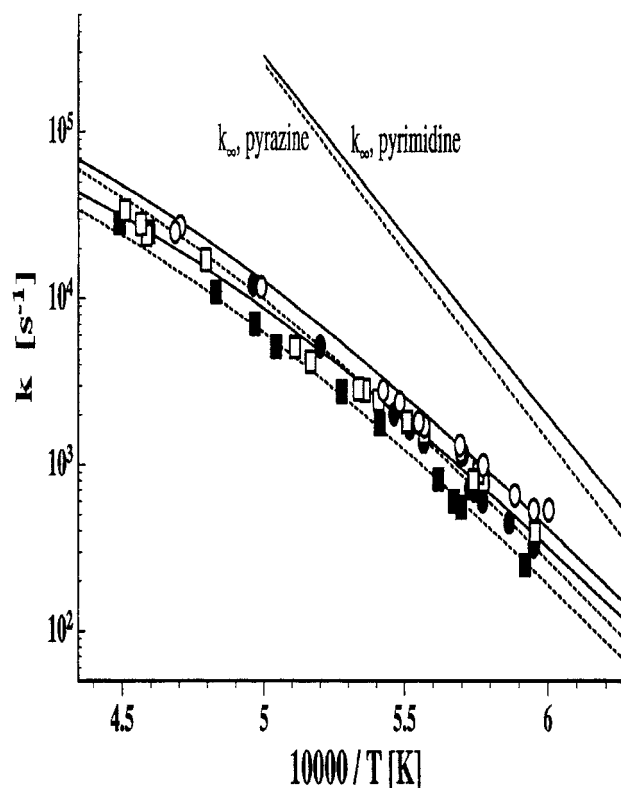


Figure 5. Arrhenius plot of first-order rate constants for the C–H fission of pyrazine, reaction 1 in Table 3, and pyrimidine, reaction 36 in Table 4: (●) pyrazine, 313–342 Torr; (■) pyrazine, 133–198 Torr; (○) pyrimidine, 266–349 Torr; (□) pyrimidine, 136–214 Torr. The solid and dashed lines illustrate the results of RRM calculations with $\langle\Delta E\rangle_{\text{down}} = 400 \text{ cm}^{-1}$ for both pyrimidine and pyrazine. The solid lines represent extrapolated values for k_{∞} , rate constants at 305 Torr (upper solid) and 165 Torr (lower solid) for pyrimidine; the dashed lines represent extrapolated values for k_{∞} , rate constants at 329 Torr (upper dashed) and 156 Torr (lower dashed) for pyrazine.

The overall rate chosen previously^{12a} for pyrazyl dissociation, $10^{12}e^{-30(\text{kcal/mol})/RT} \text{ (s}^{-1}\text{)}$, is in the falloff regime, despite the very large rate. This takes into account the fact that such a large radical can be directly formed pre-excited through thermoneutral or exothermic abstraction, reactions 8–10 of Table 3, 43–51 of Table 4, or 62–70 of Table 5, without the usual need for collisional excitation.²⁵ To reflect the same ease in the pyrimidyl dissociations, very fast rates are also adopted for the reactions in Scheme 2, namely, reactions 37–39 in Table 4.

The ring openings of the various azyl radicals formed in this pyrolysis either by dissociation or abstraction are extremely facile, with both low barriers and high entropies of reaction. An estimation of the HPL rate constant for such openings will exceed 10^{10} s^{-1} at present temperatures. Collisional activation cannot support such a large rate, and the reaction would normally fall off sharply to something near the LPL, with a much smaller rate. At the lower pressures used herein, this rate could drop to around 10^7 s^{-1} .

However, radicals formed by near-thermoneutral abstraction retain the thermal energy of the large parent molecule; most are thus formed with more than enough internal energy to open. The rates estimated herein take this situation into account; the assumed rates are larger than is reasonable for activation-restricted dissociation, but not so large as the HPL rates. This seems a reasonable compromise. This idea is relatively new; its origin and a more detailed description is available.²⁵

The species NCCHCH in eq b of Scheme 2 is one of the important radicals generated by the bond fission of its precursor radical. It is possible that this radical could undergo an H atom

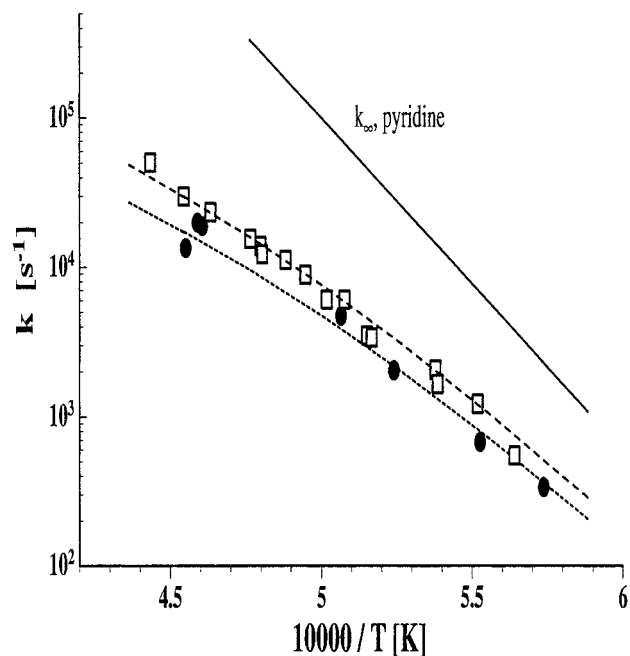


Figure 6. Arrhenius plots of first-order rate constants for C–H fission of pyridine: (□) 309–377 Torr and (●) 107–140 Torr. The solid and dashed lines illustrate the results of RRM calculations with $\langle\Delta E\rangle_{\text{down}} = 400 \text{ cm}^{-1}$, the long dashed line for 350 Torr, and the short dashed for 150 Torr. The extrapolated values for k_{∞} are also shown above the rate constant data.

migration from middle carbon to form NCCCH_2 . However, direct H–C fission from the middle carbon is much more entropy-favorable and therefore faster than H-migration, which in fact results in the formation of one of the important products, NCCCH , cyanoacetylene.

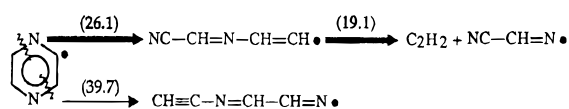
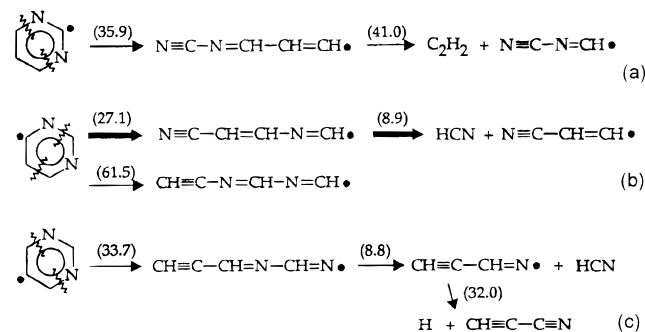
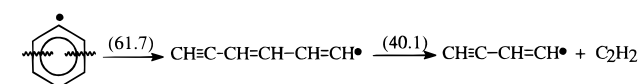
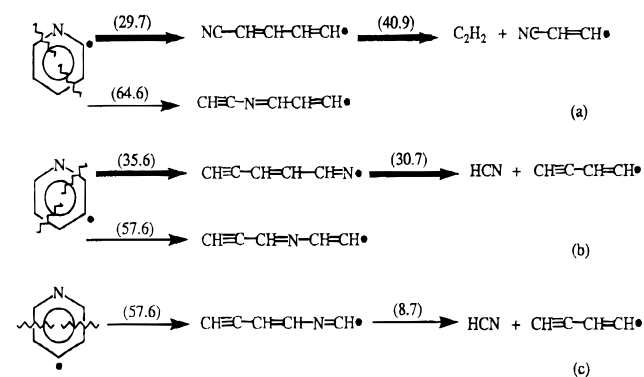
Pyridyl dissociations are similarly considered in Scheme 4. The modeling results demonstrate that it is in fact the accelerating chain and endothermicity released by the fast dissociations in these reactions and those of the subsequent linear four-membered radicals (see below) that are largely responsible for the early rise of the LS density gradients. This rise is less extreme in azine experiments than that seen in benzene pyrolysis,¹⁵ not because the reactions are slower, but because these heats of reaction are much lower than that for the phenyl dissociation in Scheme 3.

Unimolecular Dissociations of Key Small Radicals. One of the important features in azine pyrolyses is the generation of chain radicals containing a total of four C and N atoms, i.e., NCCHN , CHCHCN , and NCNCH , as shown in Schemes 1, 2, and 4. The dissociations of these radicals, reactions 3–6 in Table 3 and 40 in Table 4, largely control the overall rate of chain propagation. Unfortunately, no theoretical study of the rate of these reactions has so far been reported. The rates of these reactions are accordingly estimated using a vibration model RRM calculation chosen because these unimolecular dissociations are not simple bond fission processes; they must have barriers to their reverse reactions and local transition states. These barriers were estimated by Jursic as described previously.^{12a} Important parameters are given in Tables 7–9. The calculations, performed with a consistent value of $\langle\Delta E\rangle_{\text{down}} = 250 \text{ cm}^{-1}$ (as employed for many other molecules²⁶), demonstrate that the rate constants of these reactions are all near the low-pressure limit, but are still very fast. Together with the azyl dissociations, these decompositions assist the rise of the LS density gradients after the first microsecond by contributing additional endothermicity and promoting chain propagation.

TABLE 6: Gorin Model RRKM Parameters for Azine Dissociations: Pyridine/Pyrazine/Pyrimidine + M → *o*-Pyridyl/Pyrazyl/2-Pyrimidyl + H + M

	pyridine	pyrazine	pyrimidine
frequencies (cm ⁻¹) ^a	(374, 405, 563, 605, 700, 749, 886, 981, 981, 992, 1030, 1068, 1085, 1146, 1218, 1377, 1440, 1483, 1571, 1583, 3036, 3055, 3055, 3055), 3035, 1218, 885 ⁶	(350, 418, 602, 704, 756, 785, 960, 983, 1016, 1018, 1063, 1130, 1149, 1346, 1411, 1483, 1525, 1580, 3012, 3069, 3055), 927, 1233, 3040 ³⁶	(344, 399, 623, 678, 721, 811, 960, 980, 992, 1065, 1071, 1139, 1159, 1225, 1370, 1398, 1466, 1568, 3038, 3052, 3074), 1004, 1564, 3086 ³⁷
transition state moments of inertia (10 ⁻³⁸ gm cm ²)	2.84, 1.39, 1.45 ⁶	2.73, 1.31, 1.42 ³⁶	2.72, 1.38, 1.34 ⁴⁰
reaction path degeneracy	2	4	1
η	0.008	0.008	0.008
⟨ΔE⟩ _{down} (cm ⁻¹)	400	400	400
barrier, E _a (kcal/mol)	104.9 ± 2	103.0 ± 2	97.8 ± 2
fit of RRKM results (rms < 0.05%)			
pyridine	log k _∞ (s ⁻¹) = 16.41 - 103.6 (kcal/mol)/2.3RT		
pyrazine:	log k _∞ (s ⁻¹) = 16.72 - 103.6 (kcal/mol)/2.3RT		
pyrimidine:	log k _∞ (s ⁻¹) = 16.24 - 98.8 (kcal/mol)/2.3RT		

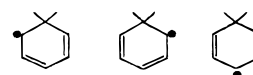
^a Frequencies in parentheses are also used for transition states.

SCHEME 1**SCHEME 2****SCHEME 3****SCHEME 4**

Additions of CN to Azine. In the earlier paper on pyrazine,^{12a} a new path to CHCCN was proposed, initiated by CN addition to the parent molecule. Here this scheme is considered in more detail and extended to the other azines.

It has been well established that H can add to the benzene ring to form the resonance-stabilized cyclohexadienyl radical (Scheme 5).²⁷⁻³⁰ The Δ_fH^o₂₉₈ of cyclohexadienyl has been determined as ~47 kcal/mol by Nicovich et al.²⁷ and Tsang.³¹ This adduct radical is in fact stabilized by delocalization of the

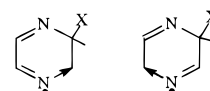
radical site around the ring via the following three resonance structures.



The resonance energy in cyclohexadienyl is estimated to be ~23 kcal/mol according to group additivity.¹⁷

It is reasonable to propose that similar additions must also occur in the azines. Specifically, various radicals "X" may add to either a N or C atom in the ring. However, because the N-X bond is much weaker than a C-X attachment, the X addition to C atom should be more important. Scheme 6 illustrates the additions of CN, H, NCCHN, and CHCHCN to the C atom of parent pyrazine.

These adduct radicals are further stabilized through two resonance structures involving the N atom lone pair, in addition to the structures analogous to those of cyclohexadienyl illustrated above.



These structures will also provide resonance energy in addition to the 23 kcal/mol derived above for cyclohexadienyl. With an additional 5 kcal/mol of resonance energy assumed for this in pyrazine, the heats of formation of the resulting adducts can be then roughly estimated by the group additivity method as 98.1 kcal/mol for CN, 67.1 for H, 129.6 for NCCHN, and 116.9 for the CHCHCN adduct. The resulting heats of reaction for each addition are also shown in Scheme 6. Due to the low concentrations of NCCHN and CHCHCN and the large negative entropy accompanying the addition of the large and unstable NCCHN and CHCHCN radicals, addition of these radicals to the pyrazine parent will hardly play an important role. Therefore, these addition reactions are neglected in the mechanisms; only the CN and H additions are recognized here. Furthermore, it is seen that CN addition is very exothermic and will ultimately lead to the formation of the important CHCHCN radical (see below). The overall result of CN addition to pyrazine, indicated by bold arrows in Scheme 7, has been included as a single step (5) in Table 3.

Based on the consideration that further decomposition of the highly activated CN addition product, cyclohexadienyl nitrile radical, could have a rate close to the high-pressure limit, the overall rate was assumed to be limited by CN addition; the

TABLE 7: Vibration Model RRKM Parameters for CHCHCN Dissociations: CHCHCN + M → CN + C₂H₂ + M (6); CHCHCN + M → H + CHCCN + M (7)

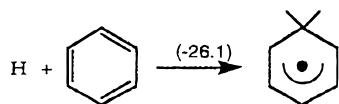
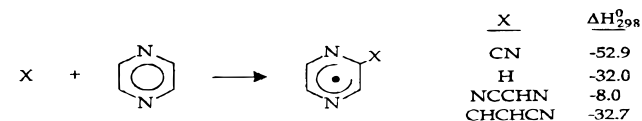
molecular frequencies (cm ⁻¹)	242, 362, 570, 683, 869, 954, 972, 1282, 1615, 2239, 3042, 3125 ³⁸	
molecular moments of inertia (10 ⁻³⁸ gm cm ²)	1.52, 1.67, 0.15 ³⁹	
	(6)	(7)
transition state frequencies (cm ⁻¹)	100, 150, 200, 500, 500, 683, 800, 1800, 2239, 3100, 3125	242, 362, 500, 500, 570, 683, 800, 1000, 1800, 2239, 3125
transition state moments of inertia (10 ⁻³⁸ gm cm ²)	3.10, 3.40, 0.15	1.52, 1.67, 0.15
I [±] /I	2.04	1.00
barrier, E _o (kcal/mol)	65.0	50.0
reaction path degeneracy	1	1
⟨ΔE⟩ _{down} (cm ⁻¹)	250	250
fits of RRKM results of 200 Torr (rms < 0.05%):		
CHCHCN + M → CN + C ₂ H ₂ + M		
log k (cm ³ /(mol s)) = 59.41 - 11.91 log T - 84.19 (kcal/mol)/2.3RT		
CHCHCN + M → H + CHCCN + M		
log k (cm ³ /(mol s)) = 46.41 - 8.55 log T - 64.04 (kcal/mol)/2.3RT		

TABLE 8: Vibration Model RRKM Parameters for NCCHN Dissociations: NCCHN + M → CN + HCN + M (3); NCCHN + M → H + C₂N₂ + M (4)

molecular frequencies (cm ⁻¹)	3000, 2243, 1609, 1386, 945, 908, 614, 333.5, 232 ³⁹	
molecular moments of inertia (10 ⁻³⁸ gm cm ²)	1.52, 1.67, 0.15 ³⁹	
	(3)	(4)
transition state frequencies (cm ⁻¹)	3150, 2243, 1800, 100, 945, 700, 50,50	2243, 1800, 800, 945, 850, 614, 350, 250
transition state moments of inertia (10 ⁻³⁸ gm cm ²)	3.10, 3.40, 0.15	1.52, 1.67, 0.15
I [±] /I	2.04	1.00
barrier, E _o (kcal/mol)	46.0	41.0
reaction path degeneracy	1	1
⟨ΔE⟩ _{down} (cm ⁻¹)	250	250
fits of RRKM results of 200 Torr (rms < 0.05%):		
NCCHN + M → HCN + CN + M		
log k (cm ³ /(mol s)) = 42.55 - 7.73 log T - 50.26 (kcal/mol)/2.3RT		
NCCHN + M → H + C ₂ N ₂ + M		
log k (cm ³ /(mol s)) = 37.75 - 6.45 log T - 44.12 (kcal/mol)/2.3RT		

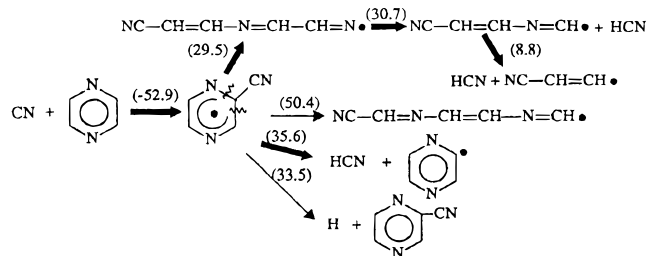
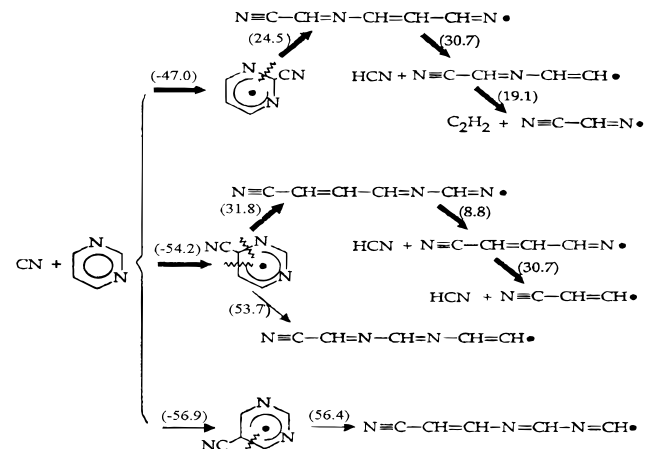
TABLE 9: Vibration Model RRKM Parameters for NCNCH Dissociation: NCNCH + M → CN + HCN + M

molecular frequencies (cm ⁻¹)	241, 358, 636, 754, 939, 1459.5, 1616.5, 2211, 3144 ³⁹
transition state frequencies (cm ⁻¹)	200, 241, 300, 754, 1459.5, 1800, 2211, 3144
molecular moments of inertia (10 ⁻³⁸ gm cm ²)	1.52, 1.67, 0.15 ³⁹
transition state moments of inertia (10 ⁻³⁸ gm cm ²)	3.10, 3.40, 0.15
reaction path degeneracy	1
I [±] /I	2.04
barrier, E _o (kcal/mol)	32.0
⟨ΔE⟩ _{down} (cm ⁻¹)	250
fit of RRKM results of 200 Torr (rms < 0.05%):	
log k (cm ³ /(mol s)) = 27.56 - 3.660 log T - 25.602 (kcal/mol)/2.3RT	

SCHEME 5**SCHEME 6**

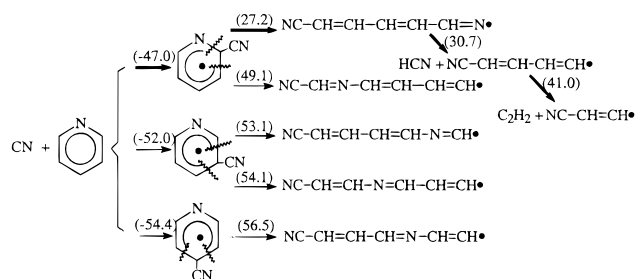
magnitude of the rate was selected to be typical of the rate of CN addition to olefins, $\sim 10^{14}$ cm³/mol-s.³²

Addition of CN to pyrimidine is similarly considered in Scheme 8. Here a group additivity analysis reveals that the three isomers have similar heats of formation, 103.1 kcal/mol for 2-, 95.8 for 4-, and 93.1 for the 5-adduct. However, ring-

SCHEME 7**SCHEME 8**

opening channels again favor the bold-arrow routes because of their low energy. The final overall consequence of these channels is either the formation of C₂H₂, HCN, and NCCHN, or 2 HCN and CHCHCN, indicated as reactions 41 and 42, respectively in Table 4. It is again assumed that CN addition

SCHEME 9



is the rate-controlling step with a rate similar to that in pyrazine. CN addition routes to pyridine are presented in Scheme 9. Clearly in Scheme 9 only the bold-arrow channels are important, and these lead to the products HCN, C₂H₂, and CHCHCN. The dominant pathways are represented by a single reaction, (61), in Table 5.

The important result in Schemes 7–9 is the formation of the CHCHCN radical, a principal precursor to the observed product CHCCN.

Discussion

(1) Initial C–H Fission. Mackie et al.⁷ and Doughty et al.^{10,11} consistently inferred a lower barrier for the initial C–H bond fissions from their pyridine and diazine experiments compared with the well-known C–H bond energy of 112 kcal/mol in benzene. This has been explained by Jones et al.⁹ as arising from the stabilization effect of the interaction of the adjacent C atom radical site with the neighboring N lone electron pair. Their computational study of the geometries of azyl radicals at the SCF/3-21G level of theory shows a noticeable shortening of the N–C bond in these radicals, which is indicative of such an interaction.

It is instructive to examine the azyl radicals as hybrids of the canonical structures illustrated in Figure 7. In addition to the benzene analogue structures (I, II, IV, V, VIII, IX, XI, XII, XIII, XIV, XVI, XVII, XVIII, and XIX), the interaction of the N lone pair with the neighboring unpaired C electron provides additional unique resonance structures, i.e., III of pyrazyl, VI and VII of 2-pyrimidyl, X of 4-pyrimidyl, and XV of *o*-pyridyl, which serve to further delocalize the unpaired electron. Therefore, the stabilization effect could also be reasonably explained, at least qualitatively, by additional contributions from these resonance structures. It seems possible to anticipate, by simply counting these additional structures, that the barrier to forming 2-pyrimidyl should be less than the barriers required to form pyrazyl, 4-pyrimidyl, and *o*-pyridyl. It also follows that the barriers involved in forming 5-pyrimidyl, *m*-pyridyl, and *p*-pyridyl are similar to the barrier for phenyl radical formation (112 kcal/mol), since additional resonance structures are not available for these radicals. The proposed C–H fission barriers for each channel inferred and derived therein are compared in Table 10.

In Table 10, the lower barrier for pyrimidine → 4-pyrimidyl is assumed to be the same as that for pyrazine dissociation. The barriers for pyrimidine/pyridine → 5-pyrimidyl/*o*-, *p*-pyridyl are the same as for benzene → phenyl. This is consistent with the discussion of additional resonance contributions of the azyls in Figure 7. The derived barriers for forming *o*-pyridyl, pyrazyl, and 2-pyrimidyl are indeed lower than the 112 kcal/mol of benzene, but not as low as the values reported by Mackie et al.⁷ and Doughty et al.^{10,11} Furthermore, the difference of the barrier reduction between pyrazine → pyrazyl and pyrimidine → 2-pyrimidyl revealed by RRKM analysis (103 vs 98 kcal/mol) clearly indicates an increased stabilization effect in

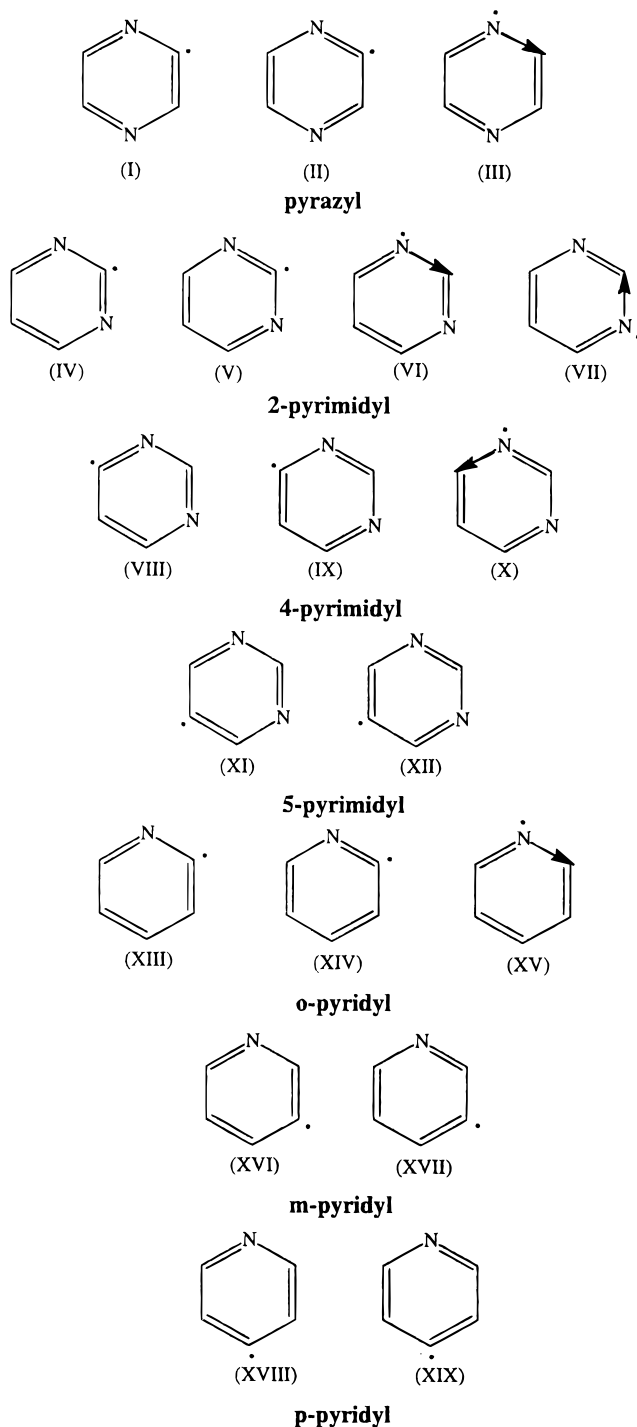
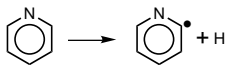
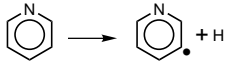
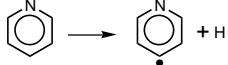
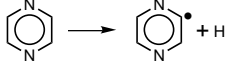
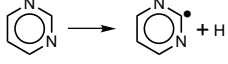
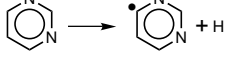
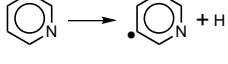


Figure 7. Resonance structures for various azyl radicals.

2-pyrimidyl, where C–H fission from ortho-C produces a radical site adjacent to two N atoms, resulting in additional delocalization. This was not seen in either the *ab initio* calculations or the single-pulse modeling (cf. Table 10). Note that the barrier of pyridine → *o*-pyridyl, 105 kcal/mol, came from an independent RRKM calculation on the refined rates of pyridine dissociation. This value, nonetheless, is quite consistent with the 103 kcal/mol for pyrazine. This can now be understood by realizing that both C–H fissions actually come from the same environment, the ortho-C, indicating a consistently reduced barrier during the formation of these radicals. All of these findings support the above discussion of proposed azyl resonance structures.

(2) Chain Mechanism. With the initiation rates defined by LS experiments and the time-resolved behavior of the stable

TABLE 10: Azine C–H Fission Barriers

C–H fission	<i>ab initio</i> ⁹	single-pulse ^{10,11}	this work
	104.0 ^a	98	105
	109.7		112
	107.8		112
	103.8	96.45	103
	104.3	95.08	98
	103.5	102.08	103
	110.7		112

^a Values in kcal/mol.**TABLE 11: Comparison of Product Yields Using the Mechanisms in Tables 3–5 with Single-Pulse Experiments^a**

species	conversion (%)	ratios	
		HCN/C ₂ H ₂	HCN/CHCCN
pyridine	6 (11) ^b	0.5 (0.5)	1.6 (1.0)
pyrazine	36 (70)	2.4 (2.3)	10.4 (8.1)
pyrimidine	47 (22)	2.7 (2.9)	9.8 (5.0)

^a Reaction conditions: 0.7% pyridine–Ar, 1450 K and 9 atm, 6×10^{-4} s; 0.3% diazine–Ar, 1450 K and 14 atm, 8.50×10^{-4} s for pyrazine and 9.25×10^{-4} s for pyrimidine. ^b Single-pulse results^{7,10,11} shown in parentheses.

products by the TOF data, the mechanisms constructed for the azine decompositions reproduce these product profiles satisfactorily over the broad temperature range 1600–2300 K. This demonstrates that the mechanisms offered herein describe the branching ratios and overall formation rates of the products very closely. As further demonstration, Table 11 compares the single-pulse data of Doughty et al.^{10,11} with our extrapolated simulation at 1450 K for the three azines. It is apparent that our model predicts lower conversions of pyridine and pyrazine than the observations, but a higher conversion of pyrimidine, both by ~50%. Compared with pyrazine conversion, the higher conversion of pyrimidine is anticipated since the previous RRKM analysis clearly shows that the rate constant of pyrimidine dissociation, when extrapolated to 1450 K, is slightly higher than that of pyrazine. A slightly faster dissociation of pyrimidine is also consistent with the results of Lifshitz in his unpublished single-pulse shock-tube study of diazine pyrolyses.³³ However, Doughty et al., had to adopt a rate constant of pyrazine almost 3 times higher than that of pyrimidine to model their high conversion of pyrazine.^{10,11} As discussed in the Introduction, the sensitivity of the single-pulse shock-tube technique to impurities in chain reactions might be responsible for their observed higher pyrazine conversion.

Despite the inconsistent prediction of azine conversion, our modeling gives a satisfactory agreement of the ratios of the main products with those reported by Doughty et al., especially for pyridine, as shown in Table 11. This again supports the product formation channels in our mechanisms.

As shown in Figure 2, a sharp early maximum of CHCCN is consistently observed at high temperatures in pyrimidine pyrolysis and also appears for the other azines, as seen in Figure

3. This has been explained through the formation of its precursor CHCHCN radical by CN addition to the azines.^{12a} This explanation was inspired in part by the reasoning that its formation must require the direct involvement of a parent azine in order to produce an early maximum, since only the reactant has a high concentration at early reaction time. The formation of CHCCN is then accomplished by subsequent loss of H from CHCHCN. The overall CN reaction with azines is thought to be limited by the rate of initial CN addition to the ring, which is then followed by fast dissociation of the chemically activated CN adduct. Many studies have indeed shown that CN reaction with olefins is dominated by exothermic addition, rather than abstraction.³²

Not only is the above mechanism of CHCHCN formation theoretically acceptable but it also describes the CHCCN TOF profiles beautifully for all the azines. As already reported in pyrazine pyrolysis,^{12a} a considerable decline in CHCCN concentration was observed in the presence of excess H₂; this behavior is also observed in the pyridine and pyrimidine experiments exhibited in Figure 3. This supports the earlier explanation for pyrazine;^{12a} the excess H₂ serves to convert CN to H atom via reaction 12, thereby reducing the contribution of the CN addition to the formation of CHCCN. The consistency of the observed drop in the initial peak in CHCCN due to H₂ addition in all the azine experiments verifies the important role of CN addition. This reaction, forming CHCCN and, at low temperatures, CH₂CHCN, is the unique contribution of CN as chain carrier.

Additional supporting evidence for our mechanism comes from the observation by Doughty et al. of an increased yield of acrylonitrile, CH₂CHCN, with excess H₂ (5%) in their single-pulse pyrazine experiments.^{10,11} Using the mechanism herein, modeling calculations reveal that CH₂CHCN concentration is increased by a factor of ~4 at 1450 K, the upper temperature end of the single-pulse experiments. This increase occurs because the dominant CH₂CHCN removal steps, reactions 17 and 18 of Table 3, are reversed by the presence of excess H₂.

C₂N₂ is another trace product in all the azine experiments, but was not quantified in the single-pulse work of Doughty et al. This is surprising given the presence of CN radicals and the inclusion of dissociation or abstraction channels in our mechanism which inevitably produce C₂N₂. Our simulation shows that the dissociation of NCCHN, reaction 4 of Table 3, is the most important source of C₂N₂ due to its low dissociation barrier of 41 kcal/mol. This channel produces a significant amount of C₂N₂, especially at the lower temperatures where there are relatively large concentrations of NCCHN radical. However, despite the importance of this C₂N₂-producing channel, the mechanisms herein are still able to hold C₂N₂ concentrations to acceptable levels for all the azines over the entire temperature range, typically $\sim 2 \times 10^{-9}$ mol/cm³, by involving the reverse of reaction 11, CN + HCN → H + C₂N₂, to destroy the excess C₂N₂. This behavior is a consequence of the large concentrations of H atoms generated in the present pyrolysis modeling.

Finally, it is worth summarizing the role of CN radical in azine pyrolyses. CN is an important chain carrier in azine decomposition, whereas in benzene pyrolysis the only significant chain carrier is the H atom. In the Doughty et al. study,^{10,11} the importance of CN as the other chain carrier in addition to H was attributed to its efficient abstraction of H atoms from diazine molecules, which was stressed to be the main reason for the observed fast overall disappearance of diazines. The present mechanisms, however, invoke the exothermic channels of CN addition to the parent azines. An analysis of the rate of

the reactions involved reveals that the real reason for the faster consumption of the azines, besides the reduced C–H fission barriers, is the ease of dissociation of all the large radicals, including the azyls and the adducts formed by CN addition to the azines.

Summary and Conclusions

This study has investigated the pyrolyses of pyrazine, pyrimidine, and pyridine using the combined LS and TOF techniques in the shock tube. The experiments cover the temperature range 1600–2300 K for pressures of 150–350 Torr. The LS gradient data clearly substantiate the chain nature of the azine pyrolyses which are initiated mainly by ring C–H fission with a well-resolved induction period. The LS data further allow an unambiguous comparison of the initial C–H fission rates for azines. RRKM fits to these rate constants, with a constant $\langle \Delta E \rangle_{\text{down}}$ of 400 cm⁻¹ and η (Gorin restriction parameter) of 0.008, both usual for large molecules, yield fission barriers of 103 ± 2 kcal/mol for pyrazine, 98 ± 2 for pyrimidine, and 105 ± 2 for pyridine. Comparing with the 112 kcal/mol for the benzene dissociation barrier, the derived barriers agree with the assessment by Doughty et al.^{10,11} that the nitrogen lone pair reduces the adjacent C–H bond energy in these heterocycles. The magnitudes of the azine barriers are attributed to the contribution of additional resonance structures of azyl radicals resulting from the interaction between the nitrogen lone pair(s) and the neighboring C–H bond.

Furthermore, substantially improved chain mechanisms, including pathways to the major products HCN, C₂H₂, CHCCN, and C₄H₂, have been proposed to successfully model the LS and TOF data of all the azines. The modeling is assisted by high-level calculations for the imine N–H bond energy, which is then used to estimate the properties of several key radicals whose dissociation rates and branching ratios largely control the formation of chain carriers. In particular, the mechanisms confirm the importance of CN in azine pyrolyses; its primary role is its highly exothermic addition to a parent azine followed by a series of very facile dissociations which finally generate the CHCHCN radical, a precursor to CHCCN and CH₂CHCN. This scheme is consistent with the TOF observation of a severe reduction of CHCCN concentration in mixtures containing initial amounts of H₂ for all the azine experiments at high temperatures. The fast overall decomposition of azines is explained in part by the reduced C–H fission barriers, but mainly by the ease of dissociation of all large secondary radicals formed here by dissociation and abstraction reactions.

Acknowledgment. Research was supported by the U.S. Department of Energy under DE-FGO2-85ER13384 (J.H.K.) and DE-FGO5-85ER13400 (R.D.K.).

References and Notes

- Axworthy, A. E.; Dayan, V. H.; Martin, G. B. *Fuel* **1987**, *57*, 29.
- Houser, T. J.; McCarville, M. E.; Biftu, T. *Int. J. Chem. Kinet.* **1980**, *12*, 555.
- Houser, T. J.; Hull, M.; Alway, R. M.; Biftu, T. *Int. J. Chem. Kinet.* **1980**, *12*, 569.
- Leidreiter, H. I.; Wagner, H. Gg. *Z. Phys. Chem. Neue Folge* **1987**, *153*, 99.
- Rawlins, W. T.; Tanzawa, T.; Schertzer, S. P.; Kreck, R. H. *Final Report to DOE*, 1983, Contract No. DEAC2280PC30392.
- Kern, R. D.; Yong, J. N.; Kiefer, J. H.; Shah, J. N. *16th Int. Symp. Shock Tubes Waves* **1987**, 43.
- Mackie, J. C.; Colket, M. B.; Nelson, P. F. *J. Phys. Chem.* **1990**, *94*, 4099.
- Kikuchi, O.; Hondo, Y.; Morihashi, K.; Nakayama, M. *Bull. Chem. Soc. Jpn.* **1988**, *61*, 291.
- Jones, J.; Bacskay, G. B.; Mackie, J. C.; Doughty, A. *J. Chem. Soc., Faraday Trans.* **1995**, *91*, 1587.
- Doughty, A.; Mackie, J. C. *J. Chem. Soc., Faraday Trans.* **1994**, *90*, 541.
- Doughty, A.; Mackie, J. C.; Palmer, J. M. *25th International Symposium on Combustion*; The Combustion Institute: Pittsburgh, 1994; p 893.
- (a) Kiefer, J. H.; Zhang, Q.; Kern, R. D.; Chen, H.; Yao, J.; Jursic, B. S. *26th International Symposium on Combustion*; The Combustion Institute: Pittsburgh, 1996; Vol. I, p 651. (b) Jursic, B. S. *J. Phys. Chem. A* **1997**, *101*, 2345.
- Kiefer, J. H.; Manson, A. C. *Rev. Sci. Instrum.* **1981**, *52*, 1392.
- Brühl, J. W. *Z. Phys. Chem.* **1897**, *22*, 481.
- Kiefer, J. H.; Mizerka, L. J.; Patel, M. R.; Wei, H. C. *J. Phys. Chem.* **1985**, *89*, 2013.
- Melius, C. F. *Calculation of Heat of Formation and Free Energy*, <http://herzberg-ca.sandia.gov/~melius/index.html>, June, 1996.
- Benson, S. W. *Thermochemical Kinetics*; John Wiley: New York, 1976.
- Harland, P. W. *Int. J. Mass Spectrom. Ion Processes* **1986**, *70*, 231.
- Dorofeeva, O. V.; Gurvich, L. V. *Thermochim. Acta* **1991**, *178*, 273.
- Dibeler, V. H.; Reese, R. M.; Franklin, J. L. *J. Am. Chem. Soc.* **1961**, *83*, 1813.
- (a) Chu, J. Y.; Nguyen, T. T.; King, K. D. *J. Phys. Chem.* **1982**, *86*, 443. (b) Stull, D. R.; Westrum, E. F., Jr.; Sinke, G. C. *The Chemical Thermodynamics of Organic Compounds*; John Wiley: New York, 1969.
- Besseris, G.; Kiefer, J. H.; Zhang, Q.; Walker, J. A.; Tsang, W. *Int. J. Chem. Kinet.* **1995**, *27*, 691.
- Tsang, W. *Combust. Flame* **1989**, *78*, 71.
- Miller, L. A.; Barker, J. R. *J. Chem. Phys.* **1996**, *105*, 1383.
- Tsang, W.; Bedanov, V.; Zachariah, M. R. *J. Phys. Chem.* **1996**, *100*, 4011.
- (a) Tsang, W.; Hampson, R. F. *J. Phys. Chem. Ref. Data* **1986**, *15*, No. 3. (b) Tsang, W. **1987**, *16*, No. 3; *17*, No. 2; *19*, No. 1; *20*, No. 2.
- Nicovich, J. M.; Ravishankara, A. R. *J. Phys. Chem.* **1984**, *88*, 2534.
- Duran, R. P.; Amorebieti, V. T.; Colussi, A. J. *J. Phys. Chem.* **1988**, *92*, 636.
- Westmoreland, P. R.; Dein, A. M.; Howard, J. B.; Longwell, J. P. *J. Phys. Chem.* **1989**, *93*, 8171.
- Ackermann, L.; Hippler, H.; Pagsberg, P.; Reihs, C.; Troe, J. *J. Phys. Chem.* **1990**, *94*, 5247.
- Tsang, W. *J. Phys. Chem.* **1986**, *90*, 1152.
- (a) Westley, F.; Frizzell, D. H.; Herron, J. T.; Hampson, R. F.; Mallard, W. J. *NIST Chemical Kinetics Database*; NIST Standard Reference Data: Gaithersburg, MD, 1993. (b) Sims, I. R.; Queffelec, J.-L.; Travers, D.; Rowe, B. R.; Herbert, L. B.; Karthaus, J.; Smith, I. W. M. *Chem. Phys. Lett.* **1993**, *211*, 461. (c) Herbert, L.; Smith, I. W. M.; Spencer-Smith, R. D. *Int. J. Chem. Kinet.* **1992**, *24*, 791. (d) Lichtin, D. A.; Lin, M. C. *Chem. Phys.* **1985**, *96*, 473.
- Lifshitz, A. Private communication, 1995.
- Ha, T. K.; Gey, E. *J. Mol. Struct. (THEOCHEM)* **1994**, *306*, 197.
- Pedley, J. B.; Naylor, R. D.; Kirby, S. P. *Thermochemical Data of Organic Compounds*, 2nd ed.; Chapman and Hall: London, 1986.
- Hewett, K. B.; Shen, M.; Brummel, C. L.; Philips, L. A. *J. Chem. Phys.* **1994**, *100*, 4077.
- Ponger, G.; Fogarasi, G. *Spectrochim. Acta* **1992**, *48A*, 243.
- Halverson, F.; Stamm, R. F.; Whalen, J. J. *J. Chem. Phys.* **1948**, *16*, 808.
- Evans, R. A.; Lorencak, P.; Ha, T.-K.; Wentrup, C. *J. Am. Chem. Soc.* **1991**, *113*, 7261.
- Fernholt, L.; Rømming, C. *Acta Chem. Acad. A* **1978**, *32*, 271.
- Herbert, L.; Smith, I. W. M.; Spencer-Smith, R. D. *Int. J. Chem. Kinet.* **1992**, *24*, 791.
- Zabarnick, S.; Lin, M. C. *J. Chem. Phys.* **1989**, *134*, 185.
- Wooldridge, S. T.; Hanson, R. K.; Bowman, C. T. *Int. J. Chem. Kinet.* **1995**, *27*, 1075.
- Kiefer, J. H.; Sidhu, S. S.; Kern, R. D.; Xie, K.; Chen, H.; Harding, L. B. *Combust. Sci. Technol.* **1992**, *82*, 101.
- Lifshitz, A.; Bidani, M.; Suslensky, A.; Tamburu, C. *J. Phys. Chem.* **1989**, *93*, 1369.
- Chase, M. W., Jr.; Davies, C. A.; Downey, J. R., Jr.; Frurip, D. J.; McDonald, R. A.; Syverud, A. N. *J. Phys. Chem. Ref. Data* **1985**, *14*, Suppl. 1.